Catal Lett (2012) 142:439–444
DOI 10.1007/s10562-012-0786-4

Comparative Study on Nano-Sized 1 wt% $Pt/Ce_{0.8}Zr_{0.2}O_2$ and 1 wt% $Pt/Ce_{0.2}Zr_{0.8}O_2$ Catalysts for a Single Stage Water Gas Shift Reaction

Dae-Woon Jeong · Hari S. Potdar · Hyun-Seog Roh

Received: 24 October 2011 / Accepted: 21 February 2012 / Published online: 7 March 2012

Abstract A comparative study on nano-sized $Pt/Ce_{0.8}Zr_{0.2}O_2$ and $Pt/Ce_{0.2}Zr_{0.8}O_2$ catalysts in a single stage water gas shift (WGS) reaction was carried out. These catalysts were prepared by impregnating 1 wt% Pt on nano-sized cubic ($Ce_{0.8}Zr_{0.2}O_2$) and tetragonal ($Ce_{0.2}Zr_{0.8}O_2$) supports. Both catalysts have been applied to WGS under identical conditions to understand beneficial effect of cubic/tetragonal phases of $Ce_{(1-x)}Zr_{(x)}O_2$. 1 wt% $Pt/Ce_{0.8}Zr_{0.2}O_2$ exhibited higher CO conversion than 1 wt% $Pt/Ce_{0.2}Zr_{0.8}O_2$. In addition, 1 wt% $Pt/Ce_{0.8}Zr_{0.2}O_2$ catalyst showed relatively stable activity with time on stream. The high activity/stability of 1 wt% $Pt/Ce_{0.8}Zr_{0.2}O_2$ catalyst was correlated to its higher Pt dispersion and easier reducibility.

Keywords $Pt/Ce_{0.8}Zr_{0.2}O_2$ · $Pt/Ce_{0.2}Zr_{0.8}O_2$ · Single stage water gas shift (WGS) · Cubic/tetragonal phase

1 Introduction

Hydrogen (H_2) is a clean energy carrier emitting only water [1, 2]. If H_2 is produced from hydrocarbons, CO should be removed from the synthesis gas mixture. Recently, the interest in the water gas shift (WGS) reaction has grown significantly as a result of recent developments in fuel cell technology [3]. WGS is a crucial step to remove CO and to produce additional H_2 from synthesis gas:

$$CO + H_2O \leftrightarrow CO_2 + H_2,\ \Delta H = -41.2 kJ/mol$$

D.-W. Jeong · H. S. Potdar · H.-S. Roh (✉)
Department of Environmental Engineering, Yonsei University, 1 Yonseidae-gil, Wonju, Gangwon 220-710, South Korea
e-mail: hsroh@yonsei.ac.kr

In general, WGS process consists of Fe_2O_3/Cr_2O_3 based high temperature shift (HTS) and $Cu/ZnO/Al_2O_3$ based low temperature shift (LTS). This process can successfully reduce CO levels to less than 1% in a large scale H_2 plant [4]. However, the conventional WGS unit is not suitable for a compact reformer due to restrictions in volume, weight and cost [5]. Thus, it is necessary to develop advanced catalysts for single stage WGS, which can do HTS and LTS at the same time.

Many attempts, therefore, have been made to develop active catalysts based on noble/transition metals supported on reducible oxides which can overcome those limitations [6–10]. Among these catalysts, Pt supported on ceria, and mixed oxides of ceria–zirconia have been identified as promising catalysts for WGS [10–14]. It is reported that both metal and support play an important role in WGS [4]. WGS is believed to occur either through an associative or a redox type mechanism [4]. In the associative mechanism, CO reacts with the bridging surface OH on the oxide to generate formate (HCOO) intermediate species [15]. By further reaction with another surface OH, the formate species is transformed into carbonate while H_2 is liberated. The simultaneous decomposition of carbonate and H_2O will generate CO_2 and restore the bridging surface OH groups. The role of the metal is to facilitate formation of OH groups on the oxide surface during the reduction process and to help to decompose intermediate formate species. In the redox type mechanism, CO is adsorbed on the metal and is oxidized at the metal/oxide interface with the formation of CO_2 [12]. The oxide surface is then reoxidized by H_2O. Thus, the nature of metal and support play crucial roles in controlling the activity/stability of the catalyst during WGS. Characteristics of $Ce_{(1-x)}Zr_{(x)}O_2$ supports not only affect adsorption properties of the Pt particles but also help to improve Pt dispersion. In addition,

the metal to support interaction is also significant for WGS [16]. Recently, it is reported that $Pt/Ce_{0.5}Zr_{0.5}O_2$ (consisting of both cubic and tetragonal phases) gave higher activity/stability than Pt/CeO_2 in WGS [9, 16].

The cubic phase of $Ce_{(1-x)}Zr_{(x)}O_2$ has higher oxygen storage capacity (OSC), reducibility and enhancement in capability of redox couple ($Ce^{4+} \leftrightarrow Ce^{3+}$) than the tetragonal phase of $Ce_{(1-x)}Zr_{(x)}O_2$ [17–19]. Therefore, it is necessary to study activity/stability of 1 wt% $Pt/Ce_{0.8}Zr_{0.2}O_2$ (cubic phase) and $Pt/Ce_{0.2}Zr_{0.8}O_2$ (tetragonal phase) in WGS. It will be useful to study the effect of the nano-sized cubic/tetragonal $Ce_{(1-x)}Zr_{(x)}O_2$ supports on controlling the reducibility and oxygen mobility [20]. Moreover, $Ce_{(1-x)}Zr_{(x)}O_2$ supports will help to reduce the formation of surface carbonate species, which deactivate the WGS catalyst [21].

The objective of the present study is to evaluate activity/stability of $Pt/Ce_{(1-x)}Zr_{(x)}O_2$ catalysts by employing ceria–zirconia supports having either cubic structure (CeO_2 rich composition) or tetragonal structure (ZrO_2 rich composition) in WGS.

2 Experimental

2.1 Catalyst Preparation

Nano-sized $Ce_{0.8}Zr_{0.2}O_2$ and $Ce_{0.2}Zr_{0.8}O_2$ supports were prepared by one step co-precipitation/digestion method [22]. Stoichiometric quantities of zirconyl nitrate (20 wt% ZrO_2 basis, MEL Chemicals) and cerium nitrate (99%, Aldrich) were dissolved in distilled water to get a solution containing Ce and Zr cations. To this solution 15 wt% KOH solution was added drop-wise at 80 °C to attain a pH of 10.5. The precipitates were aged at 80 °C for 3 days. After that, they were washed with distilled water several times and then air-dried for 2 days followed by drying at 110 °C for 6 h. The prepared supports were pre-calcined at 500 °C for 6 h. 1 wt% $Pt/Ce_{0.8}Zr_{0.2}O_2$ and $Pt/Ce_{0.2}Zr_{0.8}O_2$ catalysts were prepared by an incipient wetness impregnation method with $Pt(NH_3)_4(NO_3)_2$ (99%, Aldrich). The prepared catalysts were calcined at 500 °C for 6 h.

2.2 Characterization

The BET surface area was measured by nitrogen adsorption at −196 °C using an ASAP 2010 (Micromeritics). The average particle size was calculated from the BET data by using the equation: $d = 6/\rho A$, where ρ is the theoretical density of the material and A is the surface area of the powder. The XRD patterns were recorded using a Rigaku D/MAX-IIIC diffractometer (Ni filtered Cu−K radiation, 40 kV, 50 mA). The crystallize size was estimated using the Debye–Scherrer equation. CO-chemisorption was conducted in a BEL-METAL-3 (BEL Japan Inc.). The calcined catalyst was reduced at 400 °C for 1 h in 20% H_2/Ar flow. From the chemisorbed amount, the Pt dispersion was calculated by assuming the adsorption stoichiometry of one CO per Pt surface atom ($CO/Pt_s = 1$) [23]. Temperature programmed reduction (TPR) experiments were carried out in a BEL-CAT (BEL Japan Inc.). Typically, 0.1 g of sample was loaded into a quartz reactor. The TPR was performed using 10% H_2 in Ar with a heating rate of 10 °C min^{-1}, from 20 to 600 °C. The sensitivity of the detector was calibrated by reducing known weight of NiO.

2.3 Catalytic Reaction

Activity tests were carried out from 200 to 360 °C under atmospheric pressure in a fixed-bed micro-tubular quartz reactor with an inner diameter of 4 mm. The catalyst charge was 47 mg. T-union was employed at the exit of quartz reactor to install a thermocouple. A thermocouple was inserted into the catalyst bed to measure the reaction temperature. Prior to each catalytic measurement, the catalyst was reduced in 5% H_2/N_2 from room temperature to 400 °C at a heating rate of 3.3 °C min^{-1} and then the temperature was maintained for 1 h. Afterwards, the temperature was decreased to 200 °C. The simulated reformed gas consisted of 6.4 vol% CO, 7.1 vol% CO_2, 0.7 vol% CH_4, 43.0 vol% H_2, 28.4 vol% H_2O, and 14.4 vol% N_2. The feed $H_2O/(CH_4 + CO + CO_2)$ ratio was intentionally fixed at 2.0 because a H_2O/CH_4 ratio is typically 3 in steam reforming of methane (SRM: $H_2O + CH_4 = 3H_2 + CO$) to avoid coke formation [24–31].

A gas hourly space velocity (GHSV) of 45,515 h^{-1} was used to screen the catalysts in this study. Water was fed using a syringe pump and was vaporized at 150 °C upstream of the reactor. The product gas was chilled, passed through a trap to condense the residual water, and then analyzed on-line using an Agilent micro-gas chromatograph.

3 Results and Discussion

3.1 Characterization

Figure 1 depicts XRD patterns of $Pt/Ce_{0.8}Zr_{0.2}O_2$ and $Pt/Ce_{0.2}Zr_{0.8}O_2$ catalysts, respectively. The reflections corresponding to Pt metal particles can not be detected due to low loading content of Pt ≤ 1 wt%. All the observed reflections of $Pt/Ce_{0.8}Zr_{0.2}O_2$ catalyst are indexed to face centered cubic (fcc) fluorite structure (Fm3m space group) [22, ICDD Card No. 28-0271]. The broad symmetric peaks indicate nano-crystalline nature of $Ce_{0.8}Zr_{0.2}O_2$ support.

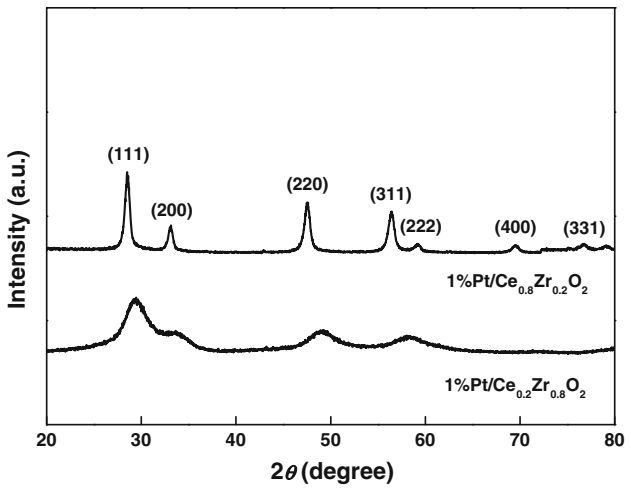

Fig. 1 XRD patterns of $Pt/Ce_{0.8}Zr_{0.2}O_2$ and $Pt/Ce_{0.2}Zr_{0.8}O_2$ catalysts

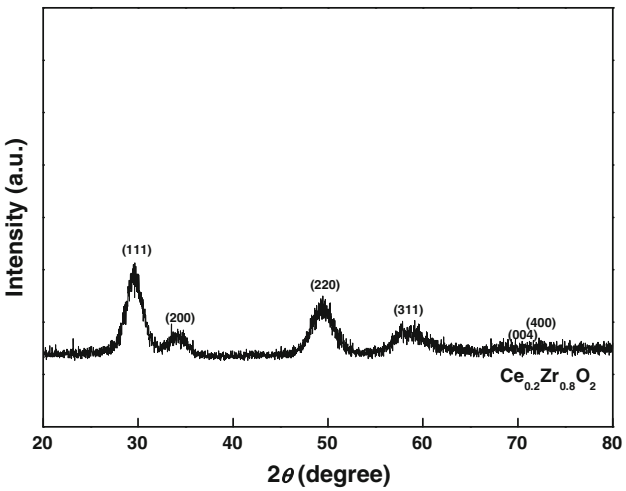

Fig. 2 XRD pattern of $Ce_{0.2}Zr_{0.8}O_2$ support calcined at 800 °C for 6 h

The calculated lattice parameter, a_0 for $Pt/Ce_{0.8}Zr_{0.2}O_2$ catalyst is 5.35 Å which agrees with the reported lattice parameter of the cubic phase of $Ce_{0.8}Zr_{0.2}O_2$ [22]. On the contrary, $Pt/Ce_{0.2}Zr_{0.8}O_2$ catalyst indicates tetragonal phase, although there is no splitting between [004] and [400] planes at $2\theta = 75°$. In addition, each peak reflection is shifted towards higher angles due to the insertion of Zr ions with the larger size (0.97 Å) into the lattice of CeO_2. This observation is consistent with the report that 25 mol% ZrO_2 or more is sufficient to obtain a fully tetragonal phase in solid solution of nano-sized ceria–zirconia [32, ICDD Card No. 80-0785]. Recently, Fuentes et al. [32] reported that nano-crystalline ceria–zirconia solid solution exhibited either cubic or tetragonal phase depending upon CeO_2 content. They applied Rietveld refinement method to know the phases present in the nano crystalline ceria–zirconia solid solution. It is established by them that the tetragonal phase is present in nano-crystalline ceria–zirconia solid solution if ZrO_2 content is $\geq$25 mol%. To confirm this issue, we heated the sample at higher temperature i.e. 800 °C for 6 h in air and XRD pattern was taken. Figure 2 shows improved crystallinity, indicating thereby homogeneity within the catalyst. Moreover, 400 reflections observed in the XRD pattern of $Ce_{0.8}Zr_{0.2}O_2$ is symmetric but the same is broad and asymmetric in that of $Ce_{0.2}Zr_{0.8}O_2$. It means that 400 reflections are split into 004 and 400 as is normally observed in the tetragonal phase of zirconia rich solid solution of ceria–zirconia. This observation suggests that the catalyst supported on $Ce_{0.2}Zr_{0.8}O_2$ has a tetragonal structure. It is well known that the addition of ZrO_2 into the lattice of CeO_2 lowers the crystallinity of ceria–zirconia solid solution.

Table 1 summarizes catalyst surface area, support surface area, and support crystallite size. Generally, the BET surface areas of catalysts are relatively lower than those of supports, indicating that the BET surface area decreases after Pt loading. The BET surface area of $Pt/Ce_{0.2}Zr_{0.8}O_2$ is twice higher than that of $Pt/Ce_{0.8}Zr_{0.2}O_2$ but the crystallite size of the tetragonal $Ce_{0.2}Zr_{0.8}O_2$ support is about four times smaller than that of the cubic $Ce_{0.8}Zr_{0.2}O_2$ support. This could be related to the tendency of the crystals to form agglomerates to lower their surface energy. It is evident from the Table 1 that the support with the higher BET surface area does not yield smaller crystallite sizes.

Table 1 Characteristics of $Pt/Ce_{0.8}Zr_{0.2}O_2$ and $Pt/Ce_{0.2}Zr_{0.8}O_2$ catalysts

Catalyst	Catalyst S.A. ($m^2\ g^{-1}$)	Support S.A. ($m^2\ g^{-1}$)	Support crystallite size (nm)
$Pt/Ce_{0.8}Zr_{0.2}O_2$	119	137	10.4[a], 6.3[b]
$Pt/Ce_{0.2}Zr_{0.8}O_2$	244	244	2.3[a], 3.9[b]

[a] Measured by XRD

[b] Calculated from BET

Table 2 CO chemisorption results of $Pt/Ce_{0.8}Zr_{0.2}O_2$ and $Pt/Ce_{0.2}Zr_{0.8}O_2$ catalysts

Catalyst	Pt dispersion (%)	Pt S.A. ($m^2\ g^{-1}$)	Pt crystallite size (nm)
$Pt/Ce_{0.8}Zr_{0.2}O_2$	66.9	1.65	1.69
$Pt/Ce_{0.2}Zr_{0.8}O_2$	55.7	1.38	2.03

Table 2 summarizes CO chemisorption results of $Pt/Ce_{0.8}Zr_{0.2}O_2$ and $Pt/Ce_{0.2}Zr_{0.8}O_2$ catalysts. It is interesting to note that Pt dispersion of $Pt/Ce_{0.8}Zr_{0.2}O_2$ (66.9%) is higher than that of $Pt/Ce_{0.2}Zr_{0.8}O_2$ (55.7%) even though the BET surface area of the former is half the value of the latter. This indicates that $Ce_{0.8}Zr_{0.2}O_2$ with cubic support

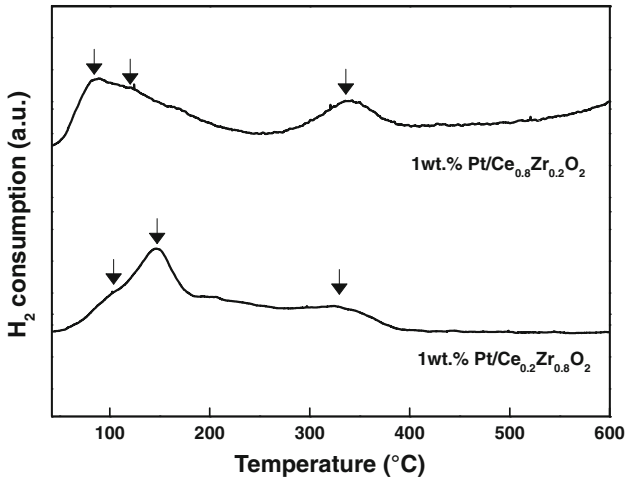

Fig. 3 TPR patterns of $Pt/Ce_{0.8}Zr_{0.2}O_2$ and $Pt/Ce_{0.2}Zr_{0.8}O_2$ catalysts

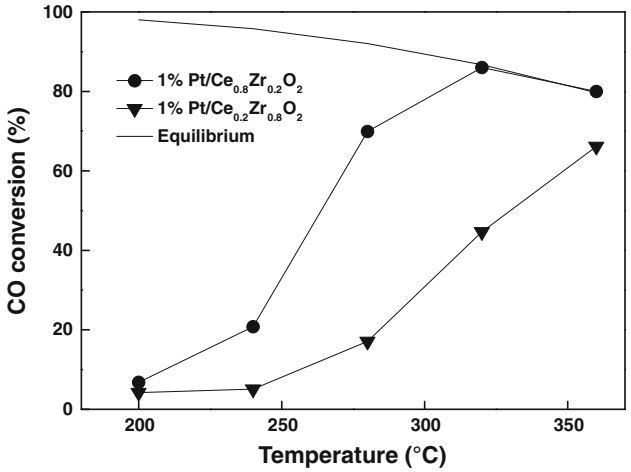

Fig. 4 CO conversion with reaction temperature over $Pt/Ce_{0.8}Zr_{0.2}O_2$ and $Pt/Ce_{0.2}Zr_{0.8}O_2$ catalysts ($H_2O/(CH_4 + CO + CO_2) = 2.0$; GHSV = 45,515 h^{-1})

helps to achieve a higher Pt dispersion. As a consequence, $Pt/Ce_{0.8}Zr_{0.2}O_2$ shows higher Pt surface area and smaller Pt crystallite size than $Pt/Ce_{0.2}Zr_{0.8}O_2$. It is interesting to note that the value of CO consumption on the $Pt/Ce_{0.8}Zr_{0.2}O_2$ i.e. 29.3 (error < 0.05) $\mu mol_{CO}/g_{cat.}$ is higher than that of 24.1 (error < 0.05) $\mu mol_{CO}/g_{cat.}$ on the $Pt/Ce_{0.2}Zr_{0.8}O_2$ catalyst under the similar treatment conditions, even though the bridging OH groups are formed during the reduction step on the ceria–zirconia catalysts.

Figure 3 shows TPR patterns of $Pt/Ce_{0.8}Zr_{0.2}O_2$ and $Pt/Ce_{0.2}Zr_{0.8}O_2$ catalysts. $Pt/Ce_{0.8}Zr_{0.2}O_2$ catalyst has three reduction peaks at 85, 120 and 340 °C, respectively. The first peak, appearing at 85 °C is attributed to the reduction of surface PtO_x species. The first peak overlaps the second peak. The second peak is assigned to the reduction of PtO_x species with an interaction with the support. The last peak at 340 °C is assigned to the reduction of bulk CeO_2 from the cubic $Ce_{0.8}Zr_{0.2}O_2$ support [33, 34]. On the other hand, $Pt/Ce_{0.2}Zr_{0.8}O_2$ catalyst shows the first peak at 100 °C with low intensity. This peak is due to the reduction of surface PtO_x species. The second prominent peak, appearing at 150 °C, is attributable to PtO_x species interacting with the support. The last peak at 330 °C is assigned to the reduction of bulk CeO_2 from tetragonal $Ce_{0.2}Zr_{0.8}O_2$ support. According to TPR results, the reduction of surface PtO_x species of $Pt/Ce_{0.8}Zr_{0.2}O_2$ is easier than that of $Pt/Ce_{0.2}Zr_{0.8}O_2$.

3.2 Reaction Results

Figure 4 depicts CO conversion profile as a function of reaction temperature over $Pt/Ce_{0.8}Zr_{0.2}O_2$ and $Pt/Ce_{0.2}Zr_{0.8}O_2$ catalysts. $Pt/Ce_{0.8}Zr_{0.2}O_2$ catalyst exhibited higher CO conversion than $Pt/Ce_{0.2}Zr_{0.8}O_2$ catalyst within the temperature range between 240 and 360 °C. This is possibly due to the presence of more irreducible ZrO_2 in $Pt/Ce_{0.2}Zr_{0.8}O_2$ catalyst and low OSC of the tetragonal $Ce_{0.2}Zr_{0.8}O_2$ phase [18, 19]. At the reaction temperature of 320 °C, $Pt/Ce_{0.8}Zr_{0.2}O_2$ catalyst reached almost equilibrium CO conversion even at the GHSV of 45,515 h^{-1}, which is 15 times higher than the typical WGS reaction condition. At this temperature, CO conversion of $Pt/Ce_{0.8}Zr_{0.2}O_2$ catalyst is about twice higher than that of $Pt/Ce_{0.2}Zr_{0.8}O_2$ catalyst. The activation energies (E_a) over $Pt/Ce_{0.8}Zr_{0.2}O_2$ and $Pt/Ce_{0.2}Zr_{0.8}O_2$ catalysts are 56 and 71 kJ mol^{-1}, respectively. To compare the reactivity of these two catalysts, turnover frequencies (TOFs) and reaction rate are given in Table 3. TOF and reaction rate of the catalyst with cubic phase at 240 °C are much higher than those of the catalyst supported on tetragonal phase. The outstanding activity of $Pt/Ce_{0.8}Zr_{0.2}O_2$ catalyst is correlated to its higher Pt dispersion, easier reducibility, lower activation energy, and higher OSC of the cubic $Ce_{0.8}Zr_{0.2}O_2$ support [18, 19].

Table 3 TOFs and reaction rate results of $Pt/Ce_{0.8}Zr_{0.2}O_2$ and $Pt/Ce_{0.2}Zr_{0.8}O_2$ catalysts

Catalyst	Temperature (°C)	Turnover frequency (s^{-1})	Reaction rate ($\mu mol_{CO}/g_{cat}$ s)
$Pt/Ce_{0.8}Zr_{0.2}O_2$	200	0.073	2.52
	240	0.223	7.65
$Pt/Ce_{0.2}Zr_{0.8}O_2$	240	0.066	1.89
	280	0.222	6.34

Figure 5 shows selectivity to CO_2 and CH_4 with reaction temperature over $Pt/Ce_{0.8}Zr_{0.2}O_2$ and $Pt/Ce_{0.2}Zr_{0.8}O_2$ catalysts. At the reaction temperature of 200 °C, the methanation reaction occurred very slightly. Above 240 °C, however, 100% selectivity to CO_2 was maintained for both

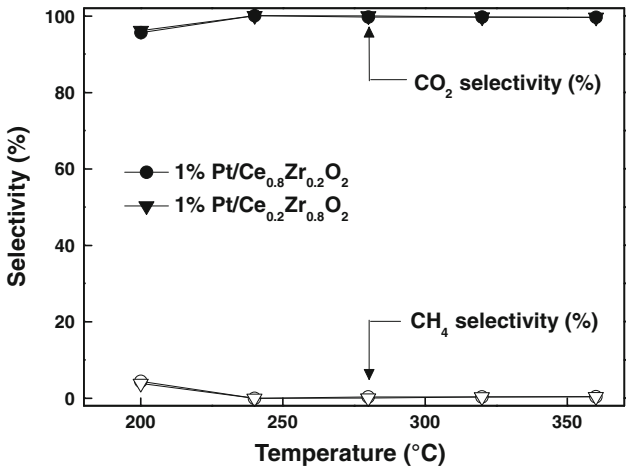

Fig. 5 Selectivity to CO_2 and CH_4 with reaction temperature over $Pt/Ce_{0.8}Zr_{0.2}O_2$ and $Pt/Ce_{0.2}Zr_{0.8}O_2$ catalysts ($H_2O/(CH_4 + CO + CO_2) = 2.0$; GHSV = 45,515 h^{-1})

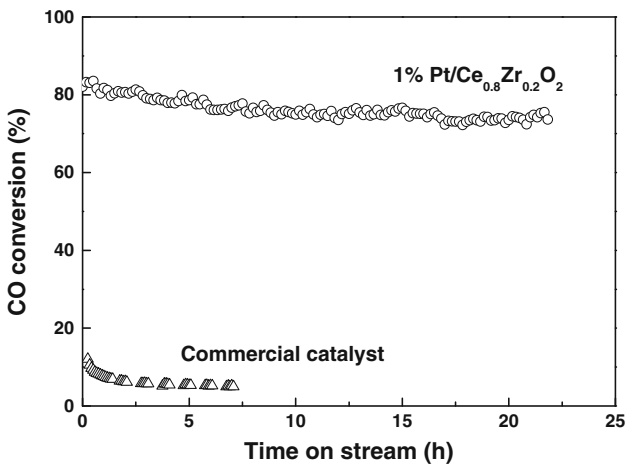

Fig. 6 CO conversion with time on stream over $Pt/Ce_{0.8}Zr_{0.2}O_2$ and commercial catalyst ($H_2O/(CH_4 + CO + CO_2) = 2.0$; $T = 320$ °C; GHSV = 45,515 h^{-1})

Table 4 Comparative data on CO conversion over $Pt/Ce_{(1-x)}Zr_{(x)}O_2$ catalysts for WGS

Catalyst	GHSV (h^{-1})	CO conversion (Reaction temp.)	Reference
1 wt% $Pt/Ce_{0.80}Zr_{0.20}O_2$	45,515	78% (300 °C)	Present work
1 wt% $Pt/Ce_{0.75}Zr_{0.25}O_2$	45,000	63% (300 °C)	[4]
1 wt% $Pt/Ce_{0.50}Zr_{0.50}O_2$	45,000	68% (300 °C)	[4]
1 wt% $Pt/Ce_{0.60}Zr_{0.40}O_2$	45,000	68% (300 °C)	[4]
1 wt% $Pt/Ce_{0.25}Zr_{0.75}O_2$	45,000	37% (300 °C)	[4]
4 wt% $Pt/Ce_{0.56}Zr_{0.44}O_2$	40,000	70% (300 °C)	[15]
4 wt% $Pt/Ce_{0.44}Zr_{0.56}O_2$	40,000	79% (300 °C)	[35]

catalysts. This indicates that both catalysts can selectively convert CO into CO_2 without the methanation reaction.

Table 4 compares reaction data on CO conversion over $Pt/Ce_{(1-x)}Zr_{(x)}O_2$ catalysts with that over $Pt/Ce_{0.8}Zr_{0.2}O_2$ catalyst tested in this study [4, 16, 35]. It should be noted that 1 wt% $Pt/Ce_{0.8}Zr_{0.2}O_2$ catalyst showed the highest CO conversion among 1 wt% $Pt/Ce_{(1-x)}Zr_{(x)}O_2$ catalysts.

To check stability of $Pt/Ce_{0.8}Zr_{0.2}O_2$ catalyst with time on stream, CO conversion data was collected for 20 h. As a reference, a commercial catalyst (Fe/Cr) was also tested under the same reaction conditions. Figure 6 shows CO conversion with time on stream over $Pt/Ce_{0.8}Zr_{0.2}O_2$ and commercial catalysts. For the $Pt/Ce_{0.8}Zr_{0.2}O_2$ catalyst, the CO conversion was decreased to 75% after 20 h. This is possibly due to the catalyst deactivation by (i) sintering of Pt particles (ii) embedding of Pt by reduced support oxide and (iii) formation of carbonate species blocking the active site at the interface region. In the case of the commercial catalyst, it showed very low CO conversion at the GHSV of 45,515 h^{-1}. This is due to the fact that conventionally the WGS reaction has been carried out at the GHSV of 3,000 h^{-1}. In another word, the commercial catalyst is not suitable for the single stage WGS, which requires high intrinsic activity at very high GHSV.

4 Conclusions

$Pt/Ce_{0.8}Zr_{0.2}O_2$ catalyst exhibits higher CO conversion than $Pt/Ce_{0.2}Zr_{0.8}O_2$ catalyst due to higher Pt dispersion, easier reducibility, lower activation energy, and higher OSC of the cubic $Ce_{0.8}Zr_{0.2}O_2$ support. Above the reaction temperature of 240 °C, $Pt/Ce_{0.8}Zr_{0.2}O_2$ catalyst shows 100% CO_2 selectivity in WGS. $Pt/Ce_{0.8}Zr_{0.2}O_2$ catalyst can be a promising candidate catalyst for the single stage WGS, which requires high intrinsic activity at very high GHSV.

Acknowledgments This work was supported by the New and Renewable Energy Technology Development Program of the Korea Institute of Energy Technology Evaluation and Planning (KETEP) grant funded by the Korea government Ministry of Knowledge Economy (2011T100200273). This research was supported by Basic Science Research Program through the National Research Foundation of Korea (NRF) funded by the Ministry of Education, Science and Technology (2010-0002521). This work is financially supported by Korea Ministry of Environment (MOE) as Human Resource Development Project for Energy from Waste and Recycling.

References

1. Park JH, Shakkthivel P, Kim HJ, Han MK, Jang JH, Kim YR, Kim HS, Shul YG (2008) Int J Hydrogen Energy 33:1845
2. Kim HJ, Shin KJ, Kim HJ, Han MK, Kim HS, Shul YG, Jung KT (2010) Int J Hydrogen Energy 35:12239
3. Farrauto R, Hwang S, Shore L, Ruettinger W, Lampert J, Giroux T, Liu Y, Ilinich O (2003) Annu Rev Mater Res 33:1

4. de Duarte Farias AM, Nguyen-Thanh D, Fraga MA (2010) Appl Catal B Environ 93:250
5. Zhu X, Hoang T, Lobban LL, Mallinson RG (2009) Catal Lett 129:135
6. Brooks C, Cypes S, Grasselli RK, Hagemeyer A, Hogan Z, Lesik A, Streukens G, Volpe AF Jr, Turner HW, Weinberg WH, Yaccato K (2006) Top Catal 38:195
7. Haryanto A, Fernando S, Murali N, Adhikari S (2005) Energy Fuels 19:2098
8. Ghenciu AF (2002) Curr Opin Solid State Mater Sci 6:389
9. Radhakrishnan R, Willigan RR, Dardas Z, Vanderspurt TH (2006) AIChE J 52:1888
10. Panagiotopoulou P, Kondarides DI (2004) J Catal 225:327
11. Roh HS, Jeong DW, Kim KS, Eum IC, Koo KY, Yoon WL (2011) Catal Lett 141:95
12. Bunluesin T, Gorte RJ, Graham GW (1998) Appl Catal B Environ 15:107
13. Querino PS, Bispo JRC, Rangel MDC (2005) Catal Today 107–108:920
14. Jeong DW, Potdar HS, Kim KS, Roh HS (2011) Bull Kor Chem Soc 32:3557
15. Ricote S, Jacobs G, Milling M, Ji Y, Patterson PM, Davis BH (2006) Appl Catal A Gen 303:35
16. Gayen A, Boaro M, de Leitenburg C, Llorca J, Trovarelli A (2010) J Catal 270:285
17. Potdar HS, Deshpande SB, Deshpande AS, Gokhale SP, Date SK, Khollam YB, Patil AJ (2002) Mater Chem Phys 74:306
18. Trovarelli A, de Leitenburg C, Dolcetti G (1997) ChemTech 27:32
19. Thammachart M, Meeyoo V, Risksomboon T, Osuwan S (2001) Catal Today 68:53
20. Kaspar J, Fornasiero P (2002) Catalysis by ceria and related Materials. In: Trovarelli A (ed) Catalytic science series. Imperials College Press, London, pp 217–243
21. Goguet A, Burch R, Chen Y, Hardacre C, Hu P, Joyner RW, Meunier FC, Mun BS, Thompsett D, Tibiletti D (2007) J Phys Chem C 111:16927
22. Potdar HS, Jeong DW, Kim KS, Roh HS (2011) Catal Lett 141:1268
23. Panagiotopoulou P, Papavasiliou J, Avgouropoulos G (2007) Chem Eng J 134:16
24. Park JC, Bang JU, Lee J, Ko CH, Song H (2010) J Mater Chem 20:1239
25. Choi SO, Moon SH (2009) Catal Today 146:148
26. Roh HS, Jun KW, Dong WS, Chang JS, Park SE, Joe YI (2002) J Mol Catal A 181:137
27. Roh HS, Jun KW, Park SE (2003) Appl Catal A Gen 251:275
28. Oh YS, Roh HS, Jun KW, Baek YS (2003) Int J Hydrogen Energy 28:1387
29. Roh HS, Jung Y, Koo KY, Jung UH, Seo YS, Yoon WL (2009) Chem Lett 38:1162
30. Roh HS, Koo KY, Jung UH, Yoon WL (2010) Curr Appl Phys 10:S37
31. Roh HS, Lee DK, Koo KY, Jung UH, Yoon WL (2010) Int J Hydrogen Energy 35:1613
32. Fuentes RO, Baker RT (2009) J Phys Chem C 113:914
33. Panagiotopoulou P, Christodoulakis A, Kondarides DI, Boghosian S (2006) J Catal 240:114
34. Hwang CP, Yeh CT (1996) J Mol Catal A 112:295
35. Boaro M, Vicario M, Llorca J, de Leitenburg C, Dolcetti G, Trovarelli A (2009) Appl Catal B Environ 88:272